Evidence for algebraic orientational order in a two-dimensional hard-core nematic

D. Frenkel and R. Eppenga*
Fysisch Laboratorium, Rijksuniversiteit Utrecht, P.O. Box 80 000, 3508-TA Utrecht, The Netherlands
(Received 22 August 1984)

We present Monte Carlo simulations on a two-dimensional (2D) fluid of N infinitely thin hard rods of length L ($N \leq 3200$). This system has an isotropic phase at low densities and a "nematic" phase at high densities. Although true long-range orientational order is not excluded *a priori*, the simulations indicate that the nematic phase has algebraic order. We find no evidence for a first-order isotropic-nematic transition; rather, all the available evidence points towards the occurrence of a disclination-unbinding transition of the Kosterlitz-Thouless type. The heat capacity C_P peaks at a density some 20% below the estimated disclination-unbinding transition point. We discuss earlier simulations on 2D nematics in the light of the current results. We have computed the virial coefficients of the hard-needle fluid up to B_5 and find that B_4 is very small, while B_5 is negative.

I. INTRODUCTION

In this paper we present a Monte Carlo study of a two-dimensional (2D) system of infinitely thin hard rods of length L (henceforth referred to as "needles"). This model system is interesting for several reasons. First of all it is the simplest purely repulsive 2D system that has a transition from an orientationally disordered state of low densities (isotropic phase) to an (at least locally) orientationally ordered state at higher densities ("2D nematic" phase). Because needles have zero proper volume no stable solid phase can exist at any finite density. The nature of the 2D nematic phase is of particular interest. About a decade ago it was shown by Straley[1] that no true long-range order (LRO) can exist in 2D nematics if the intermolecular potential is separable, i.e., if the interaction potential between two molecules can be written as

$$V(r,\Theta)=\sum_n f_n(r)g_n(\Theta)\ , \tag{1}$$

where r is the distance between the centers of mass of the molecules and Θ their relative orientation.[2] In contrast, for nonseparable interactions the existence of true LRO could not be excluded. This latter conclusion is intriguing because most 2D systems with continuous degrees of freedom lack true LRO. In a recent publication Tobochnik and Chester report a Monte Carlo study of the orientational ordering properties of 2D nematics with separable and nonseparable interactions.[3] Their results strongly suggest that the system with the nonseparable potential exhibits true LRO, unlike the system with separable intermolecular interactions. Earlier work by Vieillard-Baron[4] on another nonseparable system namely hard ellipses in two dimensions indicated that for ellipses with a ratio of long-to-short axes of $a/b=6$, the transition from isotropic to nematic phase is possibly 1° order. In contrast, for separable interactions, at least for the closely related planar spin model,[5] the transition from disordered to algebraically ordered state appears to be a continuous transition of the Kosterlitz-Thouless type.[6] The hard-needle fluid which we have investigated is an example of a nonseparable system. Hence the existence of LRO is not excluded in this system. However, as we shall discuss in Sec. III, our simulations suggest that a 2D nematic of hard needles has only quasi-LRO, i.e., the nematic order parameter vanishes in the thermodynamic limit and all order-parameter correlation functions decay algebraically.

Algebraic order is to be expected in 2D nematics if the free energy associated with collective fluctuations in the molecular orientation is of the form

$$F=\tfrac{1}{2}\int K(\nabla\theta)^2 d\mathbf{r}\ , \tag{2}$$

where $\theta(r)$ characterizes the molecular orientation with respect to a fixed axis and K is the two-dimensional Frank constant. Actually, the most general form of Eq. (2) would contain *two* Frank constants $K_{||}$ and $K_\perp$ associated with distortions parallel and perpendicular to the local director. However, on a sufficiently large length scale $K_{||}$ and $K_\perp$ are renormalized to the same value.[7] And even for smaller systems where the distinction between $K_{||}$ and $K_\perp$ is still meaningful, most predictions of the simpler elastic continuum theory described by Eq. (2) remain valid if we replace K by $(K_{||}K_\perp)^{1/2}$. Let us briefly summarize some of these predictions: First of all, the mean-square angular displacement diverges as the number of particles in the system goes to infinity

$$\langle\theta^2\rangle\approx\frac{kT}{4\pi K}\ln N\ . \tag{3}$$

As a consequence, the 2D nematic order parameter $\langle\cos(2\theta)\rangle$ vanishes as $N\to\infty$:

$$\langle\cos(2\theta)\rangle\approx aN^{-kT/2\pi K}\ . \tag{4}$$

The angular correlation functions $g_{2l}(r)$, defined as $g_{2l}(r)=\langle\cos\{2l[\theta(0)-\theta(r)]\}\rangle$, decay algebraically

$$g_{2l}(r)\approx\text{const}\times r^{-2l^2kT/\pi K}\equiv\text{const}\times r^{-\eta_{2l}}\ . \tag{5}$$

One possible mechanism for the transition from the nematic phase with quasi long-range orientational order to the isotropic phase, is through disclination unbinding.[6]

For 2D nematics this transition should occur at a universal value of the renormalized Frank constant

$$\frac{\pi K}{8kT}=1 \ . \tag{6}$$

Note that at this value of K, $\eta_2=0.25$ and $\eta_4=1$, while $\langle\cos(2\theta)\rangle\sim N^{-1/16}$. It should be stressed that other transitions even first-order ones,[8] are possible from the nematic to the isotropic phase. But no stable nematic phase is possible at values of K below the critical value given by Eq. (6). Moreover, the value of K as obtained from simulations on small systems is necessarily larger than the infinite system-size value. Hence simulations on finite systems will, if anything, overestimate the range of stability of the 2D nematic phase.

A rather different description of the isotropic-nematic (I-N) transition might apply in cases where true orientational LRO exists. In that case one may consider using the 2D equivalent of the Onsager model for the orientational ordering of 3D hard rods.[9] Kayser and Raveche[10] have analyzed the 2D Onsager model and conclude that is predicts a higher-order isotropic-nematic transition at a reduced density

$$\rho^*=(3\pi/2)\approx 4.71 \ .$$

However, as is pointed out in Ref. 10, these predictions should be viewed with some caution, because the Onsager theory neglects third- and higher-order virial coefficients, which is not warranted for 2D hard needles (see also Sec. III).

The two-dimensional equivalent of the Maier-Saupe theory[11] also predicts a continuous I-N transition, but as for hard-core systems, the strength of the "molecular field" is not simply related to molecular parameters,[12] the predictive power of this mean-field theory is rather limited.

II. COMPUTATIONAL TECHNIQUE

In this section we first describe those aspects of the Monte Carlo (MC) simulations that are either peculiar to the hard-needle system or nonstandard for some other reason. For a description of the usual MC simulation procedure we refer the reader to the literature (see, e.g., Refs. 13 and 14).

A. Monte Carlo move and overlap criterion

Acceptable configurations of the hard-needle fluid are those for which no pair of needles overlap. In a single Monte Carlo trial move both the position $\mathbf{r}_i$ and the orientation $\mathbf{u}_i$ of a needle (i) were changed. The x and y coordinates of needle i were changed by a random number $\Delta_{x\,(y)}$ uniformly distributed in the interval $-\Delta\le\Delta_{x\,(y)}\le\Delta$, while the molecular orientation, characterized by the angle θ_i was changed by a random amount $\delta\theta, -d\le\delta\theta\le d$. Both d and Δ were chosen such that the overall probability of acceptance of a trial move was $\sim 30\%$. In the actual computation the test for overlap between particles i and j consisted of two tests to see whether the intersection point of the lines through particles i and j was within $L/2$ from the center of mass of both i and j. We found it convenient to express this test in terms of unit vector $\mathbf{v}_j$ and $\mathbf{v}_j$ perpendicular to $\mathbf{u}_i$ and $\mathbf{u}_j$, respectively. The test for overlap can then be expressed as follows: Define the quantities g_i and g_j by

$$g_i\equiv(\mathbf{r}_{ij}\cdot\mathbf{v}_i)^2-\tfrac{1}{4}L^2[1-(\mathbf{v}_i\cdot\mathbf{v}_j)^2] \ , \tag{7a}$$

$$g_j\equiv(\mathbf{r}_{ij}\cdot\mathbf{v}_j)^2-\tfrac{1}{4}L^2[1-(\mathbf{v}_i\cdot\mathbf{v}_j)^2] \ , \tag{7b}$$

where $\mathbf{r}_{ij}=\mathbf{r}_i-\mathbf{r}_j$. Two needles i and j overlap if and only if both g_i and g_j are negative.

B. Pressure, density, and chemical potential

About half of the simulations were carried out at constant pressure while the rest was carried out at constant volume. A method to compute the pressure in such a constant volume simulation has been described in Ref. 15. In all cases periodic boundary conditions were employed; the shape of the unit cell was square. In order to locate possible first-order phase transitions the chemical potential was also computed using Widom's particle insertion method.[16] This method works quite well for hard needles; even at the highest densities studied ($\rho^*\approx 8.8$), the probability of acceptance of a needle thrown in at random is about 3%. During the constant pressure simulations we also kept track of the volume fluctuations. The mean-square volume fluctuations $\langle(\Delta V)^2\rangle$, are related to the isothermal compressibility χ_T by $VkT\chi_T=\langle(\Delta V)^2\rangle$ (see, e.g., Ref. 14).

C. Order parameter

The two-dimensional nematic-order parameter S of an N-particle system is defined as

$$S=\frac{1}{N}\left\langle\sum_{i=1}^{N}\cos(2\theta_i)\right\rangle \ , \tag{8}$$

where θ_i is the angle of the ith molecule with the nematic director. The order parameter and director are determined in practice by finding the eigenvalues and eigenvectors of the tensor order parameter $\underline{\underline{Q}}$:

$$Q_{\alpha\beta}=N^{-1}\sum_{i=1}^{N}[2u_\alpha(i)u_\beta(i)-\delta_{\alpha\beta}] \ , \tag{9}$$

where $u_\alpha(i)$ is the αth Cartesian coordinate of the unit vector specifying the orientation of molecule i. The eigenvalues of $\underline{\underline{Q}}$ are $\pm S$ and the corresponding eigenvectors are the nematic director and a vector perpendicular to the latter. Note that this definition of S necessarily leads to a positive order parameter, even in an isotropic phase. However, in a phase which lacks true long-range order S vanishes in the limit $N\to\infty$. In order to distinguish between true long-range order, algebraic order and short-range order it is essential to study system-size dependence of the nematic order parameter. We did this both by performing simulations on a variety of system sizes ranging from $N=30$ to $N=3200$ and by computing the order parameter for smaller subsystems formed by dividing a large system into 4, 16, or 64 blocks of equal area (see, for example, Ref. 17). Another way to obtain an estimate of the

nematic order parameter is to study the limiting behavior of the order-parameter correlation function $g_2(r) = \langle \cos\{2[\theta(0)-\theta(r)]\}\rangle$. If true LRO is present $g_2(r) \to S_2^2$ as $r \to \infty$. Of course, because finite systems were simulated it is not meaningful to look at the behavior of $g_2(r)$ for $r > D/2 = \frac{1}{2}(N/\rho)^{1/2}$, where D is the diameter of the periodic box. Note that if the system has only quasi-long-range order the estimate of S obtained from $S^2 = g_2(D/2)$ depends on the system size, $S \sim N^{-\eta_2/4}$, which is consistent with Eq. (4).

D. Disclinations

In order to test whether or not the behavior of the system close to the presumed isotropic-nematic transition is compatible with the Kosterlitz-Thouless disclination unbinding mechanism, it is useful to be able to identify disclinations. This is not straightforward because, on a microscopic scale, the director is only defined at the position of the molecules, and the latter are free to move. The first step is to extend the definition of the director in such a way that it becomes a single valued vector function defined everywhere in the periodic box. One possible definition is the following: At every point in space we define an angle $\phi(r)$ such that

$$\tan\phi(r) = \sum_i [w(\mathbf{r}-\mathbf{r}_i)\sin(2\theta_i)] \Big/ \sum_i [w(\mathbf{r}-\mathbf{r}_i)\cos(2\theta_i)] ,$$

where θ_i is the angle that characterizes the orientation of the ith molecule with respect to the x axis. $w(\mathbf{r}-\mathbf{r}')$ is a weight function chosen such that nearby moelcules dominate the director field at $\mathbf{r}$. Note that replacing θ_i by $\theta_i + \pi$ leaves ϕ unchanged. In practice we chose an antisoptropic Gaussian weight function

$$w(\mathbf{r}-\mathbf{r}_i) = \exp(-r_{||}^2/\sigma_{||}^2 - r_\perp^2/\sigma_\perp^2) ,$$

where $r_{||}$ and $r_\perp$ are the components of $\mathbf{r}-\mathbf{r}_i$ parallel and perpendicular to the orientation of the molecule under consideration. Typically, we choose $\sigma_\perp = 0.6L$ and $\sigma_{||} = 4\sigma_\perp$, thus ensuring that the "influence area" of a needle has an elongated elliptical shape rather than a circular one. Another choice of $\sigma_{||}$ and $\sigma_\perp$ would, however, not lead to qualitatively different results. In order to find disclinations we determine the value of $\phi(r)$ at a grid of points that forms a square lattice. Disclinations are identified by observing the net change in ϕ on going clockwise around an elementary "plaquette" of grid points. A positive (negative) disclination corresponds with a net change of ϕ by $+2\pi$ (-2π). Note that the orientation of the nematic director $\mathbf{n}(r)$ changes by $+\pi$ or $-\pi$ on going around an elementary disclination. The nematic director itself is however not very useful for computational purposes as it is not a single-valued function of $\mathbf{r}$ [$\mathbf{n}(\mathbf{r})$ and $-\mathbf{n}(\mathbf{r})$ are indistinguishable].

III. RESULTS

Simulations were performed on systems of N hard needles with $30 \le N \le 3200$. Most runs were carried out for $N = 50$, 200, and 800. The initial configuration from which the first few runs were started was one in which all needles were aligned but randomly positioned in the periodic box. Subsequent runs were started from previously equilibrated configurations at a higher or lower density. The phase diagram was traversed both in the direction of increasing and decreasing density in order to test for possible hysteresis effects. Most runs consisted of 2×10^4 passes (i.e., attempted moves per particle) excluding equilibration (typically 10^3 passes). But many runs in the region where nematic ordering sets in were much longer (up to 1.2×10^5 passes). Table I summarizes the relevant parameters of the simulations that were used to obtain the equation of state of hard needles (information on the order parameters will be discussed below). Figure 1 shows a plot of both the density and the chemical potential as a function of pressure. Here, and in what follows we use reduced units; $kT = 1$ and $L = 1$. At low densities one may expect that the equation of state is adequately described by the first few terms of the virial series. For hard needles the second virial coefficient is known exactly $B_2 = 1/\pi$ (in units L^2). We computed the virial coefficients B_3 through B_5 using the Monte Carlo method of Ree and Hoover.[18] The results are summarized in Table II. It is directly evident from Table II that the third and higher virial coefficients are not negligible. Hence the assumptions underlying the Onsager theory are indeed not warranted for 2D needles. A second point to note is that the fifth virial coefficient is negative. It is rather unusual for hard-core systems to have a negative virial coefficient

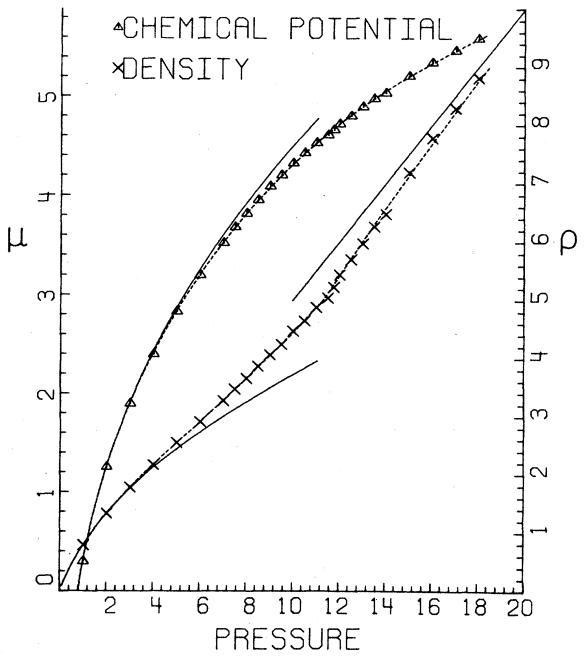

FIG. 1. Chemical potential μ (triangles) and number density ρ (crosses) of a 2D hard-needle fluid, as a function of pressure. All quantities are in reduced units. The dashed curve through the density data points is a spline fit. The dashed curve through the chemical-potential data points was obtained without adjustable parameter from the curve through the density points, using the Gibbs-Duhem relation. The two solid curves at low pressures ($P \le 11$) correspond to the five-term virial series for μ and ρ. The solid line at high pressures ($P \ge 10$) is given by the equation $\rho = P/2$ (see text).

TABLE I. Summary of thermodynamic properties as obtained by Monte Carlo simulation of a system of 2D hard needles. Column 1: P is the pressure (in units kT/L^2); column 2: ρ is the number density (units L^{-2}); column 3: μ is the chemical potential (units kT); column 4: $C_p - C_v$ (in units k); column 5: N_T is the total number of trial moves; column 6: N is the number of particles; column 7: P is the constant pressure MC, V is the constant volume MC.

P	ρ	μ	$C_p - C_v$	N_T (10^6)	N	Constant P or V
1.00	0.782	0.297	0.97	0.4	200	P
2.00	1.373	1.249	1.07	0.4	200	P
3.00	1.771	1.892	1.12	0.4	200	P
4.00	2.164	2.394	0.93	0.4	200	P
5.00	2.584	2.828	1.29	4	200	P
6.00	2.910	3.195	1.483	4	200	P
7.00	3.269	3.518	1.466	4	200	P
7.50	3.466	3.678	1.854	4	200	P
8.00	3.653	3.817	1.642	4	200	P
8.50	3.860	3.95	1.825	4	200	P
9.00	4.064	4.089	1.933	4	200	P
9.50	4.240	4.201	2.128	4	200	P
10.0	4.494	4.329	2.121	1	50	P
10.0	4.466	4.322	2.172	4	200	P
10.5	4.786	4.440	2.465	4	50	P
10.5	4.647	4.426	1.872	4	200	P
11.0	5.067	4.546	2.579	1	50	P
11.0	4.880	4.528	2.204	4	200	P
11.0	4.882		3.115	4	800	P
11.5	5.267	4.622	2.767	1	50	P
11.5	5.044	4.607	1.927	4	200	P
11.5	5.153		1.069	4	800	P
11.75	5.230	4.663	2.360	4	200	P
12.0	5.520	4.709	2.791	1	50	P
12.0	5.441	4.718	1.908	4	200	P
12.0	5.486		1.698	4	800	P
12.5	5.701	4.801	2.003	4	200	P
13.0	6.205	4.891	2.209	1	50	P
13.0	5.974	4.893	2.956	4	200	P
14.0	6.477	5.034	2.669	4	200	P
15.0	7.188	5.205	2.012	4	200	P
16.0	7.779	5.344	2.258	4	200	P
17.0	8.288	5.462	2.151	4	200	P
18.0	8.812	5.583	2.184	4	200	P
10.87	5.000				30	V
11.09	5.000			6	50	V
11.22	5.000			4	75	V
11.22	5.000			19	200	V
11.30	5.000			24	800	V
11.76	5.250			12	800	V
11.70	5.500			8	30	V
11.84	5.500			6	50	V
12.11	5.500			13	75	V
12.29	5.500			19	200	V
12.21	5.500			24	800	V
12.49	5.750			21	800	V
12.44	6.000			8	30	V
12.57	6.000			6	50	V
12.88	6.000			4	75	V
13.06	6.000			15	200	V
13.13	6.000			22	800	V
13.63	6.250			21	800	V
14.71	7.000			9	800	V
16.13	7.773			9	800	V
17.91	8.753			8	800	V

TABLE II. Virial coefficients B_2 through B_5 for 2D hard needles. Column 2: B_n in units $L^{2(n-1)}$; column 3: B_n in units B_2^{n-1}. The estimated error in the last digit is indicated between brackets.

n	B_n	B_n/B_2^{n-1}
2	$1/\pi$	1
3	0.0533(1)	0.526
4	0.00058(9)	0.0180
5	−0.00138(2)	−0.134

as low as B_5; the only other example we know of is that of thin hard platelets in 3D.[15] As can be seen from Fig. 1 the five-term virial series fits very well to the MC data for pressure $P \leq 3$. In the same pressure range the virial expression for the chemical potential coincides with the Monte Carlo results obtained by using Widom's particle insertion method. At pressures $P > 3$ the Monte Carlo data deviate significantly from the five-term virial series. In this regime we find that, for a given density, the five-term virial series always overestimates the pressure. This implies that at least one of the higher virial coefficients must be negative. At reduced pressures between $P = 11$ and 13 we observe a marked increase in equilibration times. Very long runs were needed to obtain reliable equation-of-state data in this region. The slope of the isotherm in Fig. 1 also changes rather rapidly around $P = 12$ ($\rho \approx 5.5$). In Fig. 2 we have shown typical configurations of the hard-needle fluid at four different densities between $\rho^* = 3.5$ and $\rho^* = 8.75$. As is clear from Fig. 2 there is a pronounced increase the degree of alignment of the needles at the higher densities. At pressures above $P \approx 15$ the equation of state of hard needles rapidly approaches the limiting form $P = 2\rho$. An equation of state of this form is expected when the hard-needle fluid has a high degree of orientational order on a local scale. For a derivation, see Ref. 15, where we discuss the high-density equation of state of hard platelets in three dimensions. Postponing for a moment the question whether the high-density phase has true long-range orientational order, we first look at possible evidence for a first-order phase transition between the isotropic (low-density) and "nematic" (high-density) phases. The equation of state as obtained from the MC simulations has no observable discontinuities nor is there any evidence for hysteresis. As the estimated error in the individual Monte Carlo point is of the order of 1% any discontinuous jump in the density must be appreciably less than 1%. The absence of a discontinuous density jump is consistent with the observation that the curve of μ versus P (Fig. 1) is free of discontinuous changes in slope. Of course, changes in slope are much harder to detect than discontinuities, and the smooth behavior of μ as a function of P is, in isolation, no convincing evidence. A thermodynamic quantity that is more sensitive to the nature of the phase transition is the heat capacity at constant pressure, C_P. In a hard-core system the heat capacity at constant volume, C_V, is an uninteresting quantity because it is equal to $(d/2)$ (d = dimensionality), at all densities. In contrast, C_P is sensitive to the equation of state as it is related to the compressibility

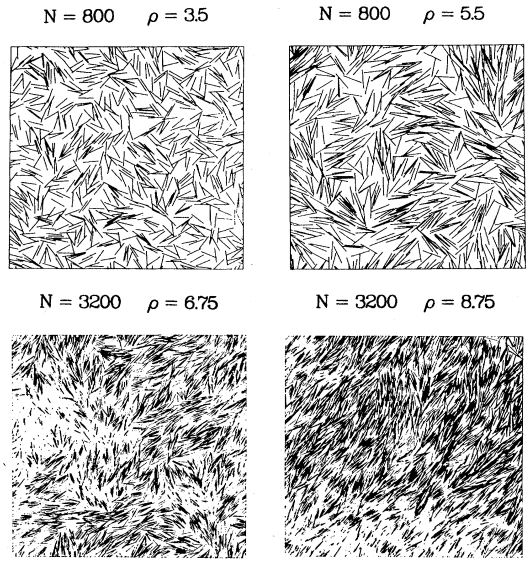

FIG. 2. Snapshots of configurations of a system of 2D hard needles at densities between $\rho = 3.5$ and 8.75. The snapshots at $\rho = 3.5$ and 5.5 show systems consisting of 800 needles; the configurations at $\rho = 6.75$ and 8.75 contain 3200 particles. Note the increase in local orientational order as the density is increased.

$$\chi_T = \rho^{-1} \left[\frac{\partial \rho}{\partial P} \right] .$$

For a 2D hard-core system we have the following expression for C_P:

$$C_P = 1 + \frac{P^2}{\rho^2} \left[\frac{\partial \rho}{\partial P} \right]_T . \tag{10}$$

For the hard-needle fluid C_P varies from 2 at very low densities (where $P = \rho$) to 3 at very high densities. The isothermal compressibility χ_T of the hard-needle gas can be obtained from the constant-pressure MC simulations through the relation

$$\frac{\langle (\Delta V)^2 \rangle}{V} = \chi_T kT .$$

Figure 3 shows the density dependence of $(C_P - C_V)$ as obtained from the mean-square volume fluctuations in constant-P MC runs. As the statistics on $\langle (\Delta V^2) \rangle$ are rather poor, the C_P points are rather noisy. The only conclusion we can draw from these data is that C_P has a peak around $\rho^* = 6$. Another method to obtain C_P is by numerical differentation of the equation of state. We did this by first performing a least-squares spline fit to the equation of state points and then differentiating this curve with respect to P. The result of this procedure depends strongly on the rigidity of the spline fit. A very smooth fit washes out all structure while an "exact" fit which goes through all data points has a derivative that fluctu-

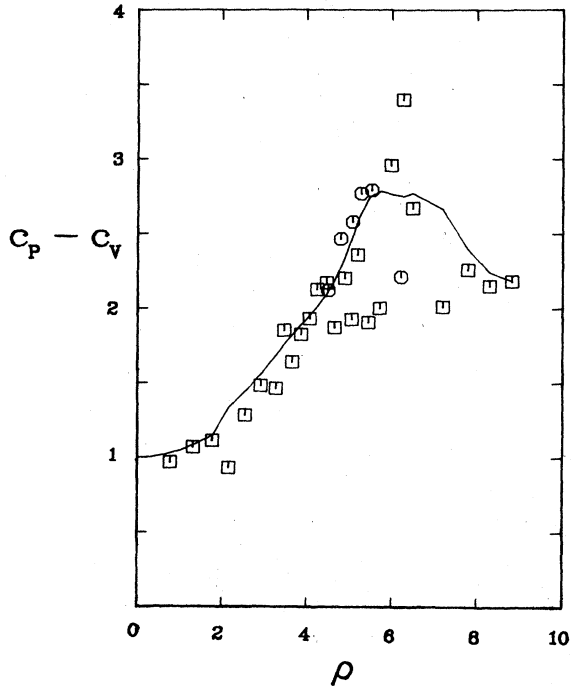

FIG. 3. C_p-C_v of a system of 2D hard needles as a function of density [see Eq. (10)]. The solid line was obtained by numerical differentiation of the equation-of-state data. The points were computed using the compressibility derived from the mean-square volume fluctuations in constant pressure runs. In the figure the results for a 200-particle system are indicated by squares; the results for a 50-particle system are shown as circles.

ates wildly. Figure 3 shows the result obtained with a spline fit that followed the data points as closely as possible without giving rise to multiple peaks in C_P. Although this criterion is of course rather arbitrary a curve for C_P results which has roughly the same width and peak height as the compressibility points. Taken together the data in Fig. 3 suggest that C_P has a finite and rather broad peak around $\rho=5.5$–6.0. This is additional evidence that the I-N transition in this system is not first order. Consistent with this picture is the observation that the histogram of volumes accumulated during the constant pressure runs never exhibited the two-peaked structure typical of weak first-order phase transitions. It should be noted that the peak in C_P occurs at a higher density than the point where the 2D Onsager model has its second-order phase transition ($\rho_0=4.71$). From the preceding discussion it is clear that the thermodynamic properties of the hard-needle fluid are not very sensitive to the onset of orientational order. In particular, on basis of the thermodynamic data alone we cannot decide what the nature of the high-density phase is, nor, indeed, if it is a distinct phase at all. Much more information can be obtained by studying the behavior of quantities directly related to the orientational ordering, in particular the nematic order parameter $S=\langle\cos(2\theta)\rangle$ and the orientational correlation functions

$$g_2(r)=\langle\cos\{2[\theta(0)-\theta(r)]\}\rangle$$

and

$$g_4(r)=\langle\cos\{4[\theta(0)-\theta(r)]\}\rangle\ .$$

Let us first consider the order parameter S. S is defined as the average positive eigenvalue of the matrix

$$Q_{\alpha\beta}=\frac{1}{N}\sum_{i=1}^{N}(2u^i_\alpha u^i_\beta-\delta_{\alpha\beta})\ . \tag{9'}$$

In a finite system, S will be small but finite even in an orientationally disordered phase. In the very dilute gas phase it is easy to show that $\langle S^2\rangle=1/N$ and hence that $S=O(1/\sqrt{N})$. At higher densities, where moleculear orientations are correlated over a finite distance ξ_2, finite size effects will be more pronounced because S will vary as $1/\sqrt{n_c}$, where n_c is the number of correlation areas: $n_c=D^2/\xi_2^2$ (where D=diameter of the periodic box). An example of the system-size dependence of S is shown in Fig. 4. This figure clearly shows that the onset of orientational order is not abrupt and, moreover, occurs at different densities for different system sizes. It should be stressed that long runs are needed to get a reliable estimate of S once orientational order starts to develop throughout the periodic box. In particular for the larger systems ($N=800,3200$), S may fluctuate appreciably on "time scales" of 30 000 passes or more. For example, for a well-equilibrated system of 800 needles at $\rho=5.5$ we found the following values for S in subsequent runs: $S=0.141$ (2.2×10^4 passes), $S=0.129$ (1.5×10^4 passes), and $S=0.216$ (1.5×10^4 passes). If we assume that the typical "relaxation time" for fluctuations in S scales as D^2 then the number of passes to obtain S with a given accuracy also scales as D^2, i.e., as N. The total number of Monte Carlo trial moves then goes as N^2. It is clear from this rough estimate that computation times become prohi-

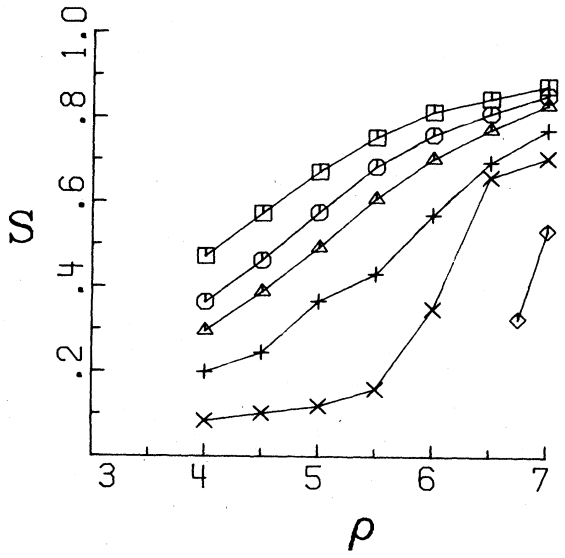

FIG. 4. Apparent nematic order parameter $S=\langle\cos(2\theta)\rangle$ as a function of density. The different curves refer to different system sizes. Squares: $N=30$; circles: $N=50$; triangles: $N=75$; pluses: $N=200$; crosses: $N=800$; diamonds: $N=3200$.

TABLE III. System-size dependence of the apparent nematic order parameter at densities between $\rho=4.0$ and 7.0. Values of the order parameter are tabulated for system consisting of $N=30$, 50, 75, 200, and 3200 particles. The length of the simulations (in millions of attempted moves) is indicated between brackets. The last three columns contain the result of a least-squares fit of the system-size dependence of the order parameter of the form $S=aN^{-b}$. The best fit values of b, a, and the regression coefficient r of the fit are tabulated.

ρ	$N=30$	N_T (10^6)	$N=50$	N_T (10^6)	$N=75$	N_T (10^6)	$N=200$	N_T (10^6)	$N=800$	N_T (10^6)	$N=3200$	N_T (10^6)	b	a	r
4.0	0.471	(10)	0.363	(8)	0.295	(9)	0.198	(22)	0.084	(21)			0.50	2.6	0.999
4.5	0.572	(10)	0.462	(8)	0.387	(9)	0.245	(20)	0.102	(23)			0.43	2.5	0.999
5.0	0.670	(17)	0.575	(14)	0.491	(11)	0.365	(47)	0.119	(46)			0.33	2.1	0.993
5.5	0.752	(18)	0.682	(14)	0.607	(20)	0.429	(38)	0.159	(46)			0.24	1.7	0.97
6.0	0.811	(18)	0.757	(14)	0.701	(11)	0.568	(31)	0.348	(41)			0.16	1.4	0.99
6.5	0.842	(10)	0.807	(9)	0.770	(7)	0.693	(16)	0.658	(19)			0.095	1.17	0.995
7.0	0.872	(10)	0.850	(9)	0.828	(7)	0.769	(16)	0.703	(12)	0.532	(12)	0.058	1.06	0.994
6.75									0.720	(3)	0.325	(1)			

bitively long if we aim to obtain reliable information about S for systems larger than $N=800$. Data on the nematic order parameter for different system sizes have been collected in Table III. We can try to fit the system-size dependence of S to a power law of the form $S=aN^{-b}$. The results of such a fit for system sizes with $30\leq N\leq 800$ are summarized in the last three columns of Table III. In this fit we have weighted the MC data points with a factor proportional to the number of passes and inversely proportional to the system size. For densities $\rho\leq 4.0$ we observe that $b\approx\frac{1}{2}$ which is the result we expect for an isotropic system. At higher densities b becomes less than $\frac{1}{2}$. It should be stressed, however, that even at highest densities studied, we always find that the order parameter decreases with increasing system size. Table IV contains information on the block-size dependence of the block-averaged order parameter S, and S^2, and S^4 at densities $\rho\geq 7$. At these densities the molecular orientation is correlated throughout the periodic box, at least for the system sizes studied ($N\leq 3200$). We find that the exponents b_1, b_2, and b_4 for $N=800$ and $N=3200$ are comparable though the values tend to be somewhat larger for the larger system. At this point it is useful to recall that if elastic continuum theory may be used to describe long-wavelength orientational fluctuations in the 2D nematic, the exponent b is related to the effective Frank constant K: $b=kT/2\pi K$. The exponents b_2 and b_4 describing the N dependence of $\langle S^2\rangle$ and $\langle S^4\rangle$ are in that case related to b by $b_2=2b$ and $b_4=4b$. We observe that at $\rho=8.75$ the relation $b=b_2/2=b_4/4$ is satisfied within computational accuracy for both $N=800$ and $N=3200$. For $N=800$ $b_2/2b=1.00$, $b_4/4b=1.08$, while for $N=3200$ $b_2/2b=1.02$ and $b_4/4b=1.06$. In contrast, at $\rho=7$ the relation between b, b_2, and b_4 starts to deviate from the predictions of the 2D elastic continuum theory: $b_2/2b=0.94$, $b_4/4b=0.87$ ($N=3200$). The system is unstable against spontaneous disclination unbinding if $\pi K/kT<8$, i.e., $b>\frac{1}{16}$, $b_2>\frac{1}{8}$, and $b_4<\frac{1}{4}$. Hence the data in Tables III and IV suggest that at densities $\rho\leq 7$ no stable nematic with quasi-LRO can exist. The existence of a nematic with true LRO is very unlikely in view of the very pronounced system-size dependence of the nematic order parameter. Additional evidence that the system is isotropic for $\rho\leq 7$ comes from the decay of the orientational correlation function

$$g_2(r)=\langle\cos\{2[\theta(0)-\theta(r)]\}\rangle$$

and $g_4(r)=\langle\cos\{4[\theta(0)-\theta(r)]\}\rangle$. As discussed in Sec. II elastic continuum theory predicts an algebraic decay of $g_{2l}(r)$ in the nematic phase

$$g_2(r)\sim r^{-\eta_2},\quad g_4(r)\sim r^{-\eta_4}$$

with $\eta_2=2kT/\pi K$ and $\eta_4=8kT/\pi K$. Spontaneous disclination unbinding occurs if $\eta_2>\frac{1}{4}$, $\eta_4>1$. Figures 5–7 show a log-log plot of $g_2(r)$ and $g_4(r)$ versus r at densities both above and below $\rho=7$. We observe that at the highest densities the decay of both functions is algebraic while at densities $\rho\leq 7$ the decay is faster than algebraic. The values of η_2 and η_4 (Table V) are found to be larger

TABLE IV. Effect of block averaging on the apparent nematic order parameter at densities between $\rho=7$ and $\rho=8.75$ for systems of 800 ($\rho=7.5$ and 8.75) and 3200 ($\rho=7$, 7.5, and 8.75) particles. The first four rows contain the values of the order parameter S for the full system (1/1) and subsystems with an area equal to $\frac{1}{4}$, $\frac{1}{16}$, and $\frac{1}{64}$ of the periodic box. The numbers between parentheses indicate the total number of attempted Monte Carlo moves (in millions). Rows 5–7 contain the parameters of a least-squares fit of the (sub)system order parameter $S(N)$ to an expression $\ln S(N)=a-b\ln N$, where N is the average number of particles in the subsystem; r is the regression coefficient of the fit. Rows 8–14: the same for the mean-square order parameter. Rows 15–21: the same information for the mean fourth power of the order parameter. Row 22: value $\langle b\rangle$ obtained by averaging b, $b_2/2$, and $b_4/4$. Row 22: value of $\pi K/8kT$ deduced from $\langle b\rangle=kT/2\pi K$. Spontaneous disclination unbinding is expected to take place at $\pi K/8kT=1$.

		$\rho=7$	$\rho=7.5$		$\rho=8.75$	
		$N=3200$	$N=800$	$N=3200$	$N=800$	$N=3200$
S	(1/1)	0.532 (12)	0.732 (7)	0.732 (47)	0.864 (4)	0.820 (24)
	(1/4)	0.549 (11)	0.758 (4)	0.750 (35)	0.872 (4)	0.832 (21)
	(1/16)	0.632 (11)	0.796 (4)	0.769 (35)	0.888 (4)	0.844 (21)
	(1/64)	0.7333 (11)	0.864 (4)	0.821 (35)	0.919 (4)	0.873 (21)
r		0.999	0.998	0.989	0.994	0.991
b		0.105	0.035	0.044	0.013	0.023
a		1.11	0.91	0.97	0.93	0.95
S^2	(1/1)	0.284	0.537	0.550	0.747	0.673
	(1/4)	0.312	0.572	0.564	0.761	0.692
	(1/16)	0.428	0.646	0.598	0.791	0.714
	(1/64)	0.562	0.759	0.681	0.848	0.765
r_2		0.999	0.995	0.991	0.994	0.991
b_2		0.198	0.083	0.087	0.026	0.047
a_2		1.22	0.89	0.96	0.88	0.92
S^4	(1/1)	0.082	0.294	0.304	0.558	0.453
	(1/4)	0.108	0.337	0.323	0.582	0.480
	(1/16)	0.219	0.442	0.372	0.632	0.515
	(1/64)	0.355	0.602	0.482	0.728	0.595
r_4		0.996	0.994	0.993	0.994	0.992
b_4		0.365	0.186	0.177	0.056	0.098
a_4		1.5	0.91	0.97	0.79	0.87
$\langle b\rangle$		0.098	0.041	0.044	0.013	0.024
$\pi K/8kT$		0.64	1.52	1.42	4.81	2.60

TABLE V. Results of fit of the orientational correlation functions $g_2(r)\equiv\langle\cos\{2[\theta(0)-\theta(r)]\}\rangle$ and $g_4(r)\equiv\langle\cos\{4[\theta(0)-\theta(r)]\}\rangle$ to an expression of the form $\ln g_{2l}(r)=a-\eta_{2l}\ln r$, for $4.5\le\rho\le8.75$ and $N=800$ and 3200. Columns 3–6 contain the best-fit values of η_2 and η_4 and the corresponding regression coefficients. N_T (column 7) is the total number of attempted Monte Carlo moves. Column 8 contains the estimate of $\pi K/8kT$ obtained from η_2 and η_4 using the relation $\eta_2=\eta_4/4=2kT/\pi K$. Column 9 gives typical values for the number of disclinations per 800 particles.

ρ	N	η_2	r	η_4	r	N_T (10^6)	$\pi K/8kT$	N_D
4.5	800	2.4	0.93	2.6	0.92	11		23
5.0	800	1.4	0.99	2.0	0.82	4		16
5.5	800	1.9	0.81	2.3	0.94	12		15
6.0	800	0.72	0.99	1.61	0.95	11		4.5
6.5	800	0.36	0.998	1.65	0.90	16	0.65	2.5
6.75	3200	1.2	0.99	3.9	0.94	1	0.23	3.5
7.0	800	0.20	0.98	0.78	0.996	9	1.27	1
	3200	0.39	0.99	1.77	0.98	11	0.60	0.5
7.5	800	0.16	0.98	0.78	0.999	4	1.41	0
	3200	0.15	0.99	0.61	0.99	23	1.65	0
8.75	800	0.050	0.97	0.203	0.96	4	4.96	0
	3200	0.059	0.99	0.252	0.99	21	4.10	0

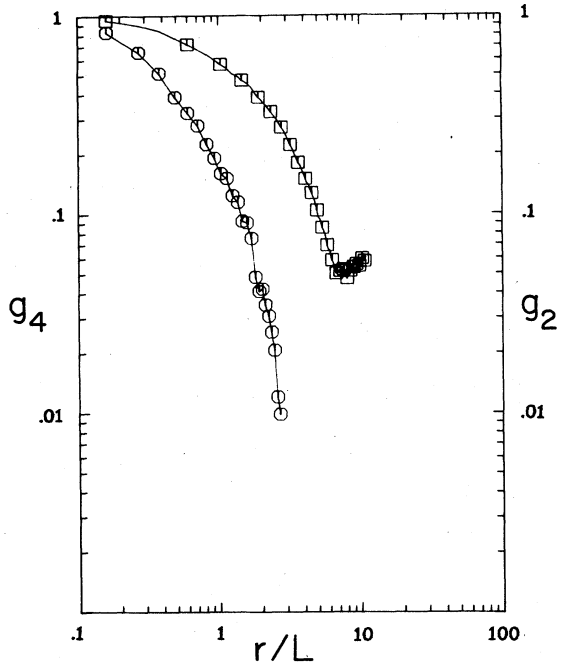

FIG. 5. Log-log plot of $g_2(r)=\langle\cos\{2[\theta(0)-\theta(r)]\}\rangle$ (squares), and $g_4(r)=\langle\cos\{4[\theta(0)-\theta(r)]\}\rangle$ (circles) as a function of r (in units L). The system size is $N=3200$, the density $\rho=6.75$. Note the residual secondary maximum in $g_2(r)$ which is a consequence of slow equilibration. As can be seen from the figure the decay of both $g_2(r)$ and $g_4(r)$ is faster than algebraic.

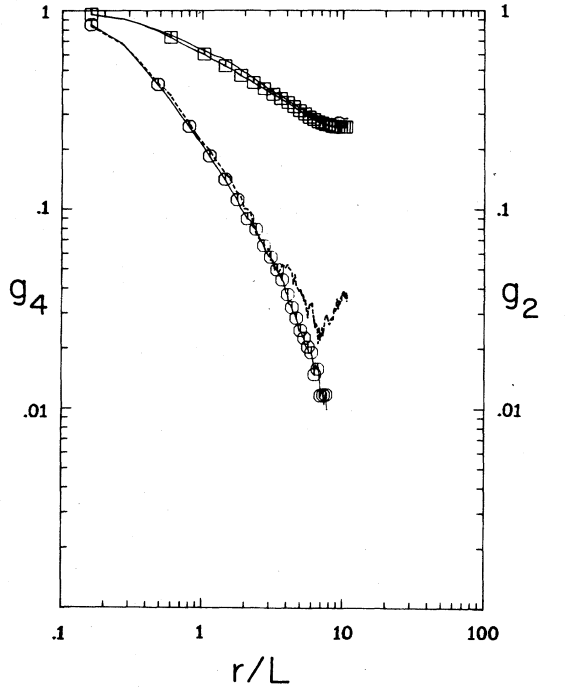

FIG. 6. Log-log plot of $g_2(r)=\langle\cos\{2[\theta(0)-\theta(r)]\}\rangle$ (squares), and $g_4(r)$ is $\langle\cos\{4[\theta(0)-\theta(r)]\}\rangle$ (circles) as a function of r (in units L). The system size is $N=3200$, the density $\rho=7.00$. The points shown were obtained after a fairly long run ($\sim 4\times 10^3$ passes). In addition we show the result obtained in the run immediately preceding the above run [dashed curve for $g_4(r)$, solid curve for $g_2(r)$]. From the figure it is clear that the secondary maximum in $g_4(r)$ disappears on equilibration; $g_2(r)$ relaxes somewhat slower than $g_4(r)$.

than the critical value for disclination unbinding at all densities $\rho \leq 7$. We should add that for the 3200-particle systems, which were prepared by quadrupling a previously equilibrated 800-particle configuration, excessively long runs were needed to allow the initial correlations between the four subsystems to decay. These correlations showed up as a secondary maximum in $g_2(r)$ and $g_4(r)$ at $r=D/2$. The relaxation times involved in the decay of this secondary maximum were in some cases longer than we could afford to wait (for an example, see Fig. 6). For these cases the exponents η_2 and η_4 were obtained by performing the fit on $g_2(r)$ and $g_4(r)$ only for values of r where these functions were decreasing; in all cases points with $r<2L$ were excluded from the fit because at very short distances local ordering effects will dominate. We find that fluctuations in the orientational correlation functions occur on the same time scale as fluctuations in the total-order parameter. In this respect the present system seems to behave differently from the model systems studied by Tobochnik and Chester.[3] These authors note that the statistics on $g_2(r)$ tend to be much better than the statistics on S.

Combining the information on the effective Frank constant as obtained from b_1, b_2, b_4, η_2, and η_4 (see Tables IV and V), we find that the data are consistent with the existence of a phase with algebraic orientational order for $\rho \geq 7.5$ and an isotropic phase for $\rho \leq 7$. Note that the thermodynamic data do not exhibit unusual behavior in the vicinity of the presumed I-N transition; the phase transition occurs at a density which is some 20% higher than the density where C_P has its maximum. At densities below $\rho \approx 4.0$, $g_2(r)$, and $g_4(r)$ are very short ranged, they do not fit well to a simple exponential. This can be seen from Figs. 8 and 9. For this reason it was not possible to determine correlation lengths of the orientational order in the isotropic phase. Taken together, the behavior of the hard-needle system is strongly reminiscent of the 2D planar-spin model which almost certainly undergoes a Kosterlitz-Thouless disclination unbinding transition. If indeed a disclination unbinding transition occurs in the hard-needle system it should be possible to observe a marked increase in the number of topological defects in the region where the heat capacity has its maximum. We have employed the construction described in Sec. II to visualize disclinations. This method suffers from a certain degree of aribtrariness because of the artificial coarse graining of the director field. As a consequence the absolute number of disclinations, which is rather sensitive to the degree of coarse graining, has little meaning. Still we can compare different configurations that have been analyzed in the same way. We find that the total number of defects is too small to be observed for $\rho \geq 7.5$ and increases rapidly, but not discontinuously, as the density is

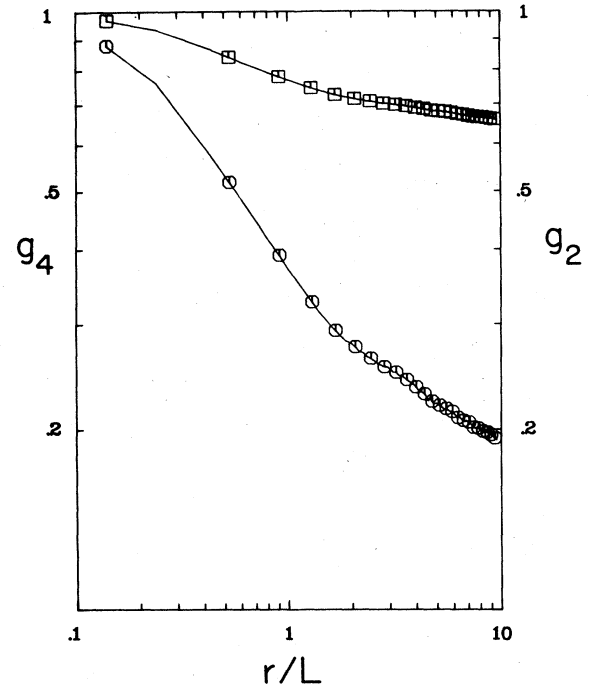

FIG. 7. Log-log plot of $g_2(r)=\langle\cos\{2[\theta(0)-\theta(r)]\}\rangle$ (squares) and $g_4(r)=\langle\cos\{4[\theta(0)-\theta(r)]\}\rangle$ (circles) as a function of r (in units L). The system size is $N=3200$, the density $\rho=8.75$. The decay of both $g_2(r)$ and $g_4(r)$ appears to be algebraic for distances $(r/L)>1$.

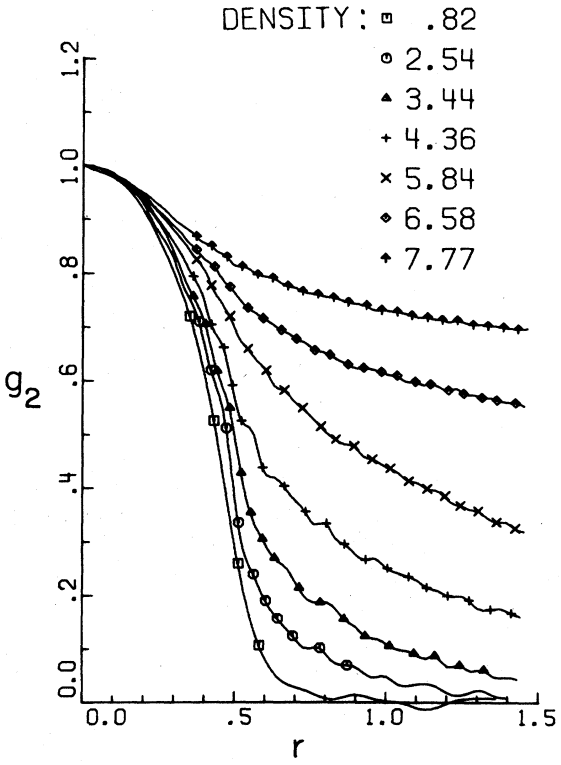

FIG. 8. Short-range behavior of $g_2(r)=\langle\cos\{2[\theta(0)-\theta(r)]\}\rangle$ as a function of r (in units L). Note that for densities $\rho\leq 5.84$, $g_2(r)$ has decayed to a value less than e^{-1} within $1.5L$.

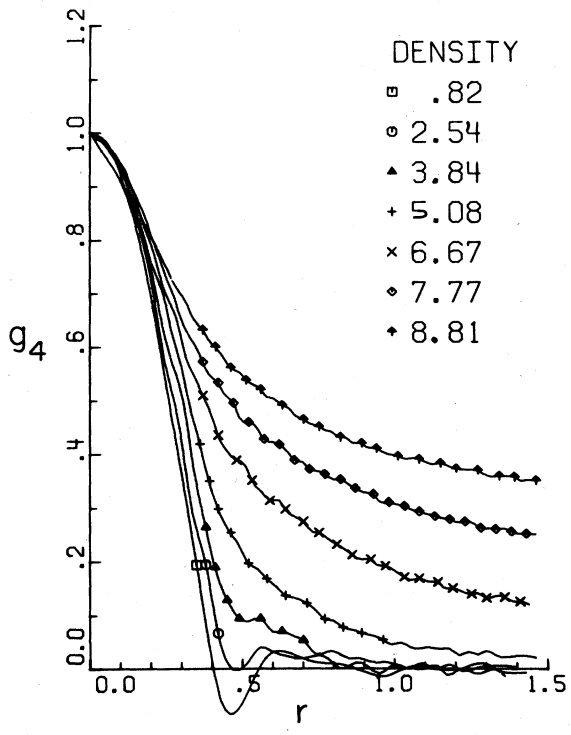

FIG. 9. Short-range behavior of $g_4(r)=\langle\cos\{4[\theta(0)-\theta(r)]\}\rangle$ as a function of r (in units L). Note that for densities $\rho\leq 5.08$, $g_4(r)$ decays to a value less than e^{-1} within $1L$.

decreased. Around $\rho=7$ we observed no free disclination, but this is hardly surprising in view of the "small" system sizes studied. Some typical defect structures are shown in Fig. 10. Typical numbers for the defect concentration have been collected in Table V. These numbers are only meant as an indication as they are based on the results for one or two snapshots. As was mentioned in the beginning of this paper hard needles do not solidify at finite densities. As a consequence we expect to observe only short-range translational order at all densities studied. That this is indeed the case can be seen from Fig. 11 where we have plotted the radial distribution function, $g(r)$, at a number of densities. Two things should be noted. First of all, $g(r)$ is almost completely featureless for $r>L$. Secondly, the onset of local orientational order is reflected in a strong increase in $g(r)$ for $r<L$. This is understandable because the centers of mass of parallel needles can come arbitrarily close. Let us briefly summarize our findings for the hard-needle fluid. Our observations are compatible with the following picture. At low densities the hard-needle fluid is in an isotropic phase in which orientational correlations die out over a distance smaller than the length of the needle. At high densities ($\rho\geq 7.5$) we find a 2D nematic phase with algebraic order. For densities $\rho\leq 7$ this ordered phase becomes absolutely unstable with respect to disclination unbinding. On the basis of the present data we tentatively conclude that a Kosterlitz-Thouless (KT) disclination-unbinding transition takes

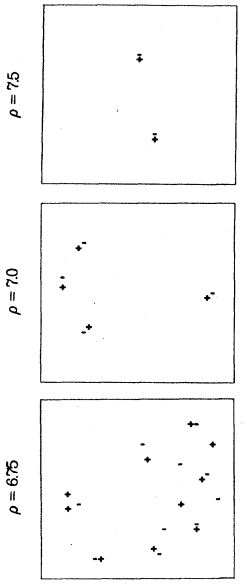

FIG. 10. Typical defect structure of a fluid of 2D hard needles at $\rho=6.75$, 7.0, and 7.5. Positive and negative disclinations are indicated by + and −, respectively. Note that for $\rho \geq 7$ disclination pairs appear to be tightly bound.

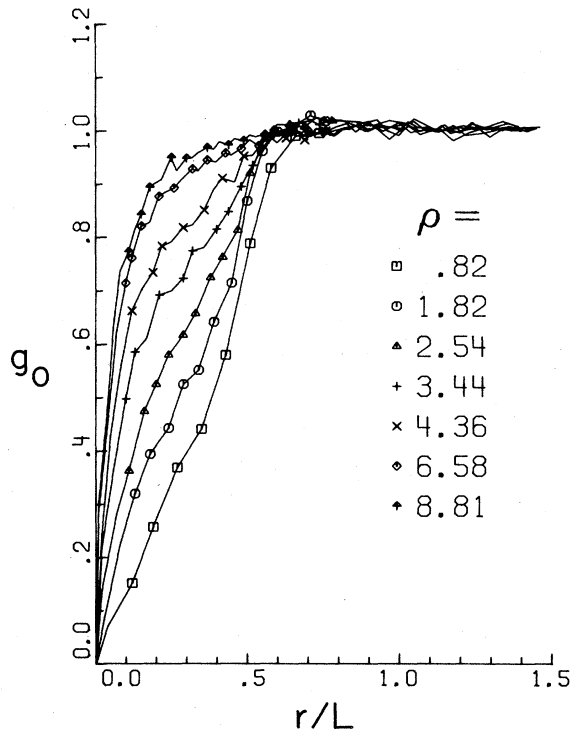

FIG. 11. Short-range behavior of the radial distribution function $g(r)$ as a function of r (in units L). Note that at all densities $g(r)$ is completely featureless for $r>L$. At short distances ($r<0.5L$) $g(r)$ increases strongly as local orientational ordering sets in.

place around $\rho \approx 7.25$. But it is possible that simulations on large systems will result in a further renormalization of the effective Frank constant. This would shift the KT transition to still higher densities. In the vicinity of the *I-N* transition we find no evidence for any anomalies of the thermodynamic properties, rather we observe a broad peak in C_P at a density some 20% lower. We stress that although the Straley argument does not exclude true LRO in systems with nonseparable interactions it does not exclude algebraic order either. To our knowledge the present simulations constitute the first example of algebraic orientational order in a molecular model system with translational degrees of freedom and nonseparable interactions.

It is natural to ask whether the hard-needle system behaves qualitatively different from the hard-ellipse system studied by Vieillard-Baron.[4] We recall that Vieillard-Baron found evidence for a first-order isotropic-nematic transition at a reduced density $\rho/\rho_0=0.563\pm0.008$. ($\rho_0$ is the density of close packing), in a system of 170 hard ellipses with a ratio of the major to the minor axis of $a/b=6$. In order to investigate the nature of the nematic phase in this system we carried out several runs on a system of 186, 744, and 2976 hard el-

TABLE VI. Data on the effective Frank constant of a N-particle hard-ellipse system ($a/b=6$), $N=186$, 744, and 2976 at $\rho=0.6\rho_0$ (ρ_0 is the density of close packing). Rows 1–21: block averages of S, S^2 and S^4, as in Table IV. Rows 22 and 23: exponents η_2 and η_4, as in Table V. Row 24: $\pi K/8kT$ obtained by combining the information on b, b_2, b_4, η_2, and η_4. Note that $\pi K/8kT<1$. Note, moreover, that K is renormalized to smaller values as the system size increases. The total number of attempted Monte Carlo moves is indicated over every column.

		$N=186$ ($N_T=9\times10^6$)	$N=744$ ($N_T=8\times10^7$)	$N=2976$ ($N_T=3.8\times10^7$)
S_2	(1/1)	0.666	0.489	0.400
	(1/4)	0.720	0.500	0.402
	(1/16)	0.798	0.617	0.431
	(1/64)	0.903	0.726	0.591
r		0.999	0.98	0.98
b		0.072	0.138	0.206
a		0.95	1.05	1.30
S_2^2	(1/1)	0.447	0.243	0.160
	(1/4)	0.528	0.263	0.162
	(1/16)	0.653	0.407	0.200
	(1/64)	0.835	0.559	0.379
r_2		0.999	0.98	0.99
b_2		0.150	0.290	0.424
a_2		0.94	1.24	1.9
S_2^4	(1/1)	0.207	0.062	0.026
	(1/4)	0.296	0.082	0.027
	(1/16)	0.459	0.199	0.049
	(1/64)	0.733	0.362	0.178
r_4		0.999	0.99	0.99
b_4		0.310	0.598	0.868
a_4		0.98	1.97	5.0
η_2		0.32	0.41	0.68
η_4		1.38	1.52	2.2
$\pi K/8kT$		0.79	0.50	0.33

lipses ($a/b=6$) at $\rho/\rho_0=0.6$, i.e., at a density some 7% higher than Vieillard-Barons's I-N transition. We performed the same analysis of the system-size dependence of the order parameter as described before and we also studied the behavior of the orientational correlation functions $g_2(r)$ and $g_4(r)$. The results of this analysis have been collected in Table VI. The data show a pronounced system-size dependence of the order parameter, while both $g_2(r)$ and $g_4(r)$ decay monotonically as a function of r. Analyzing the data in terms of an effective Frank constant we find that, for the largest system size, $\pi K/8kT\approx 0.33$. At this value the nematic phase is unstable with respect to disclination unbinding. This finding is corroborated by the fact that we observe a high defect concentration in the hard-ellipse fluid at $\rho/\rho_0=0.6$. Hence the present analysis suggests that the I-N transition observed by Vieillard-Baron is in fact related to a peak in the compressibility in the isotropic phase, similar to what we observe in the hard-needle fluid between $\rho=5.5$ and 6. We have not analyzed higher density points of the hard ellipse system and hence we do not know the nature of the true nematic phase in this system. The absence of any discontinuities in the thermodynamic properties of the hard-ellipse system between $\rho/\rho_0=0.563$ and 0.83 makes it unlikely that the I-N transition is first order. A rough estimate of the location of the point where spontaneous disclination unbinding becomes possible can be obtained in the following way. As can be seen from Table IV the order parameter in the nematic phase of the hard-needle fluid has a system-size dependence of the form $S=a\ N^{-b}$ with $a\approx 1$, which is reasonable as S must be 1 for $N=1$. If we assume that a $a=1$ for the hard-ellipse system we find that at the disclination unbinding point $S=N^{-1/16}$. For $N=170$ this yields $S=0.73$. The data in Ref. 4 show that S reaches this value at $\rho/\rho_0\approx 0.65$. Due to the renormalization of K, the true disclination-unbinding instability is probably at a somewhat higher density. It thus appears that the I-N transition in the hard-ellipse system need not be qualitatively different from that observed in the hard-needle fluid, although more work is needed to sort this out. The nonseparable ellipsoidal Lennard-Jones system studied by Tobochnik and Chester remains the only example of a 2D liquid crystalline system which appears to exhibit true LRO, but we should add that we have been unable to reproduce their results.

---

*Present address: Philips Research Laboratory, P.O. Box 80 000, 5600-JA Eindhoven, The Netherlands.

[1]J. P. Straley, Phys. Rev. A **4**, 675 (1971).
[2]M. Romeiro. J. Math. Phys. **19**, 802 (1978).
[3]J. Tobochnik and G. V. Chester, Phys. Rev. A **27**, 1221 (1983).
[4]J. Vieillard-Baron, J. Chem. Phys. **56**, 4729 (1972).
[5]J. Tobochnik and G. V. Chester, Phys. Rev. B **20**, 3761 (1979).
[6]J. M. Kosterlitz and D. Thouless, J. Phys. C **6**, 1181 (1973).
[7]D. R. Nelson and R. A. Pelcovits, Phys. Rev. B **16**, 2191 (1977).
[8]E. Domany, M. Schick and R. H. Swendsen, Phys. Rev. Lett. **52**, 1535 (1984).
[9]L. Onsager, Ann. N.Y. Acad. Sci. **51**, 627 (1949).
[10]R. F. Kayser and H. J. Raveché, Phys. Rev. A **17**, 2067 (1978).
[11]J. Y. Denham, G. R. Luckhurst and C. Zannoni, Mol. Cryst. Liq. Cryst. **60**, 185 (1980).
[12]T. J. Sluckin and P. Shukla, J. Phys. A **16**, 1539 (1983).
[13]J. P. Valleau and S. G. Whittington, in *Modern Theoretical Chemistry: Statistical Mechanics A*, edited by B. J. Berne (Plenum, New York, 1977), Vol. V, p. 137; J. P. Valleau and G. H. Torrie, *ibid.*, p. 169.
[14]J. P. Hansen and I. R. McDonald, *Theory of Simple Liquids* (Academic, London, 1976), p. 45.
[15]R. Eppenga and D. Frenkel, Mol. Phys. **52**, 1303 (1984).
[16]B. Widom, J. Chem. Phys. **39**, 2808 (1963).
[17]K. Binder, in *Applications of the Monte Carlo Method,* Vol. XXXVI of *Topics in Current Physics* (Springer, Berlin, 1984).
[18]F. H. Ree and W. G. Hoover, J. Chem. Phys. **40**, 939 (1963).